Increased catecholamine secretion contributes to hypertension in TRPM4-deficient mice

Ilka Mathar,[1] Rudi Vennekens,[2] Marcel Meissner,[1] Frieder Kees,[3] Gerry Van der Mieren,[4] Juan E. Camacho Londoño,[1] Sebastian Uhl,[1] Thomas Voets,[2] Björn Hummel,[5] An van den Bergh,[4] Paul Herijgers,[4] Bernd Nilius,[2] Veit Flockerzi,[1] Frank Schweda,[6] and Marc Freichel[1]

[1]Experimentelle und Klinische Pharmakologie und Toxikologie, Universität des Saarlandes, Homburg, Germany. [2]Department of Molecular and Cellular Biology, Laboratory of Ion Channel Research, Campus Gasthuisberg, Leuven, Belgium. [3]Institut für Pharmakologie, Universität Regensburg, Regensburg, Germany. [4]Laboratory for Experimental Cardiac Surgery, Campus Gasthuisberg, Leuven, Belgium. [5]Klinische Chemie und Laboratoriumsmedizin, Universitätsklinikum des Saarlandes, Homburg, Germany. [6]Institut für Physiologie, Universität Regensburg, Regensburg, Germany.

Hypertension is an underlying risk factor for cardiovascular disease. Despite this, its pathogenesis remains unknown in most cases. Recently, the transient receptor potential (TRP) channel family was associated with the development of several cardiovascular diseases linked to hypertension. The melastatin TRP channels TRPM4 and TRPM5 have distinct properties within the TRP channel family: they form nonselective cation channels activated by intracellular calcium ions. Here we report the identification of TRPM4 proteins in endothelial cells, heart, kidney, and chromaffin cells from the adrenal gland, suggesting that they have a role in the cardiovascular system. Consistent with this hypothesis, *Trpm4* gene deletion in mice altered long-term regulation of blood pressure toward hypertensive levels. No changes in locomotor activity, renin-angiotensin system function, electrolyte and fluid balance, vascular contractility, and cardiac contractility under basal conditions were observed. By contrast, inhibition of ganglionic transmission with either hexamethonium or prazosin abolished the difference in blood pressure between *Trpm4*$^{-/-}$ and wild-type mice. Strikingly, plasma epinephrine concentration as well as urinary excretion of catecholamine metabolites were substantially elevated in *Trpm4*$^{-/-}$ mice. In freshly isolated chromaffin cells, lack of TRPM4 was shown to cause markedly more acetylcholine-induced exocytotic release events, while neither cytosolic calcium concentration, size, nor density of vesicles were different. We therefore conclude that TRPM4 proteins limit catecholamine release from chromaffin cells and that this contributes to increased sympathetic tone and hypertension.

Introduction

Regulation of blood pressure is a complex integrated response involving various organ systems, including vasculature, heart, kidneys, adrenal glands, and the CNS. These systems modulate key determinants of blood pressure, such as cardiac output, fluid volumes, and peripheral vascular resistance. Impaired blood pressure regulation may lead to essential hypertension, the most common cardiovascular disease and a major risk factor for stroke, end-stage renal disease, and heart disease (1). Despite the importance of hypertension as a cause of disease, its pathogenesis remains unknown in nearly 95% of cases. Most of the genes identified so far affect renal hemodynamics, ion and water transport, and regulation of hormones and humoral agents (2). Recently, the large family of transient receptor potential (TRP) channels has been associated with the development of several cardiovascular diseases, including cardiac hypertrophy and vascular contractility (3, 4). Proteins of the TRP family exhibit a 6-transmembrane domain architecture and form cation channels activated by, among others, temperature, receptor stimulation, chemical agonists, or possibly mechanical forces. In this way, they may contribute directly to transplasmalemmal Ca^{2+} influx and/or influence intracellular Ca^{2+} concentration ($[Ca^{2+}]_i$) indirectly by setting the membrane potential or regulating Ca^{2+} release from intracellular organelles (5–7). Depending on the cell type, TRP channel–mediated changes in cellular Ca^{2+} homeostasis can lead to alterations in vascular and cardiac contractility, neurotransmitter release, secretion of vasoactive hormones, mineral absorption, and body fluid balance (3).

In recent years, 28 mammalian TRP-related proteins have been cloned, which are divided in 6 subfamilies (8): the classical TRPs (TRPC1–7); the vanilloid receptor TRPs (TRPV1–6); the melastatin TRPs (TRPM1–8); the mucolipins (TRPML1–3); the polycystins (TRPP1–3); and ankyrin transmembrane protein 1 (TRPA1). Although there is evidence that multiple TRP isoforms are relevant for the regulation of vascular contractility, including TRPC1, TRPC3, TRPC4, TRPC5, TRPC6, TRPV1, TRPV4, TRPM4, TRPM7, TRPP2, and TRPA1 (4, 9, 10), the contribution to systemic blood pressure regulation was analyzed only for 3 TRP isoforms so far, TRPC6, TRPV1, and TRPV4. Due to the lack of a specific pharmacology for most TRPs, studies to unravel the roles of TRP channels currently rely on experiments using transgenic animals. *Trpc6*$^{-/-}$ mice show on average a moderate elevation of about 7 mmHg in basal mean arterial blood pressure (MAP) measured in conscious mice using a telemetric system, enhanced agonist-induced and myogenic contractility of isolated vessels, and higher basal cation entry in vascular smooth muscle cells, which was explained by an increased TRPC3-mediated basal cation entry and membrane depolarization (11). Measurements performed under pentobarbital anesthesia showed that *Trpv1*$^{-/-}$ mice exhibit no difference in basal blood pressure, but activation of TRPV1 channels by intravenous application of capsaicin leads to a

Conflict of interest: The authors have declared that no conflict of interest exists.
Citation for this article: *J Clin Invest.* 2010;120(9):3267–3279. doi:10.1172/JCI41348.

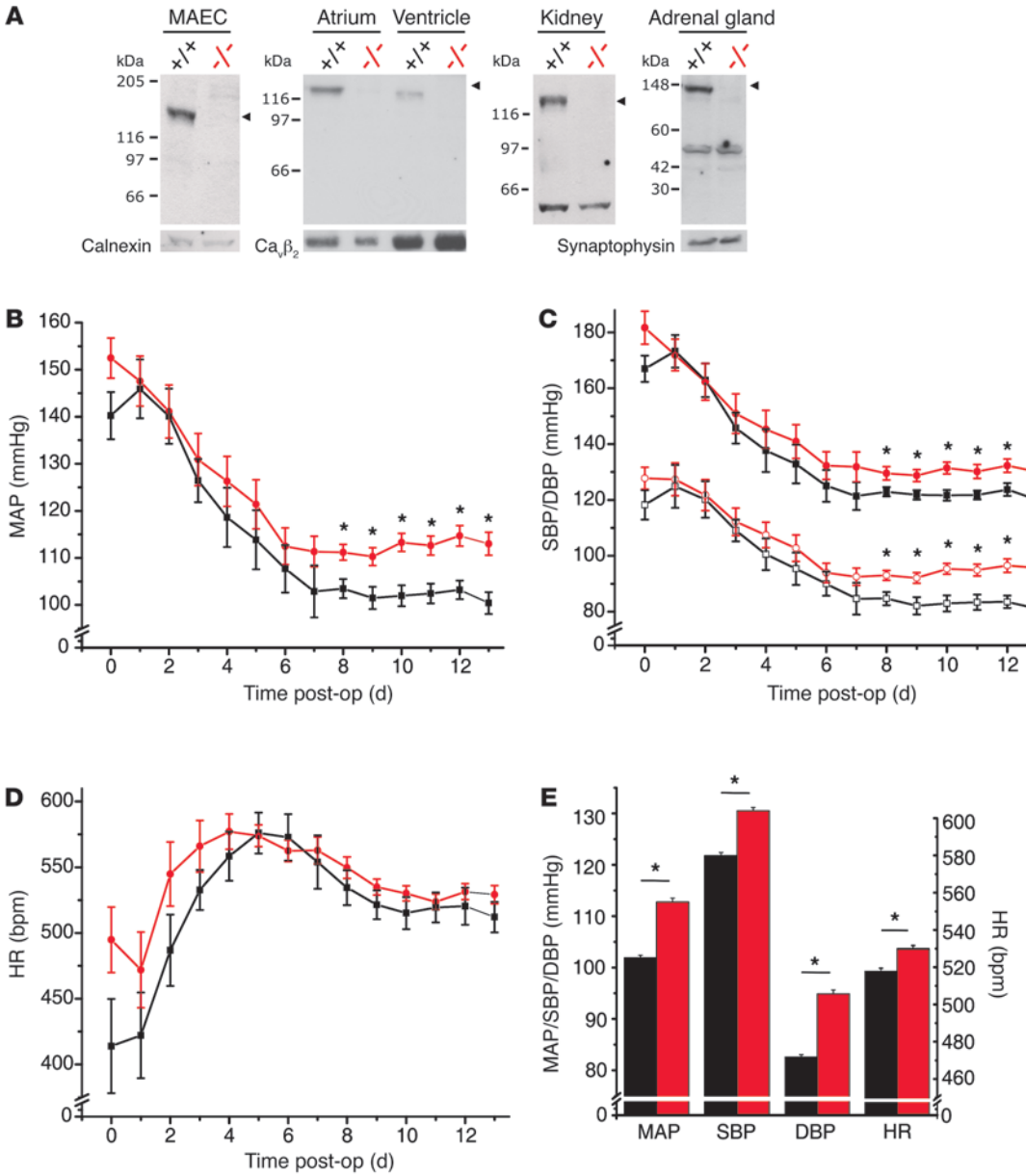

Figure 1

Elevated blood pressure in TRPM4-deficient mice. (**A**) Western blot of protein fractions from aortic endothelial cells (MAEC), atrium, ventricle, kidney, and adrenal gland of WT (+/+) and TRPM4-deficient (–/–) mice using TRPM4-specific antibody 578. (**B**–**E**) Time course of MAP (*$P < 0.01$, **B**), SBP (*$P < 0.05$) and DBP (*$P < 0.01$) (**C**), and HR (**D**) in WT (black, $n = 7$–13) and *Trpm4*$^{-/-}$ mice (red, $n = 8$–15) after implantation of the blood pressure transmitter. (**E**) Averaged MAP, SBP, and DBP from the period of day 9 to day 13 after implantation (*$P < 0.01$).

transient blood pressure increase in WT mice that is not observed in *Trpv1*$^{-/-}$ mice (12). Also, inactivation of TRPV4 in mice does not lead to changes in basal blood pressure (13, 14), although TRPV4 channels are critical regulators of Ca^{2+} entry in vascular endothelial cells (15) and shear stress–induced vasodilation (16–18).

It might be anticipated that another member of the TRPM subfamily, TRPM4, plays a role in the cardiovascular system. TRPM4 and its closest structural relative, TRPM5, exhibit distinct properties within the TRP channel family. They form nonselective cation channels that are activated by intracellular Ca^{2+} and carry Na^+ as the main charge carrier under physiological conditions (19–23). We recently showed that TRPM4 proteins act as Ca^{2+}-activated nonselective cation channels and critically reduce the driving force for Ca^{2+} influx in mast cells, thereby limiting antigen-induced mast cell activation and anaphylactic reactions (24). In addition to mast cells, *Trpm4* mRNA was also detected in several murine cell types or organs of the cardiovascular system, including heart, endothelial cells, and kidney (20, 25), and in rat cerebral artery and smooth muscle cells (26). In the heart, *Trpm4* mRNA was amplified from cells of the sinoatrial node (27) and Purkinje fibers (28), and cardiac TRPM4 expression was reported to be upregulated in spontaneously hypertensive rats (29).

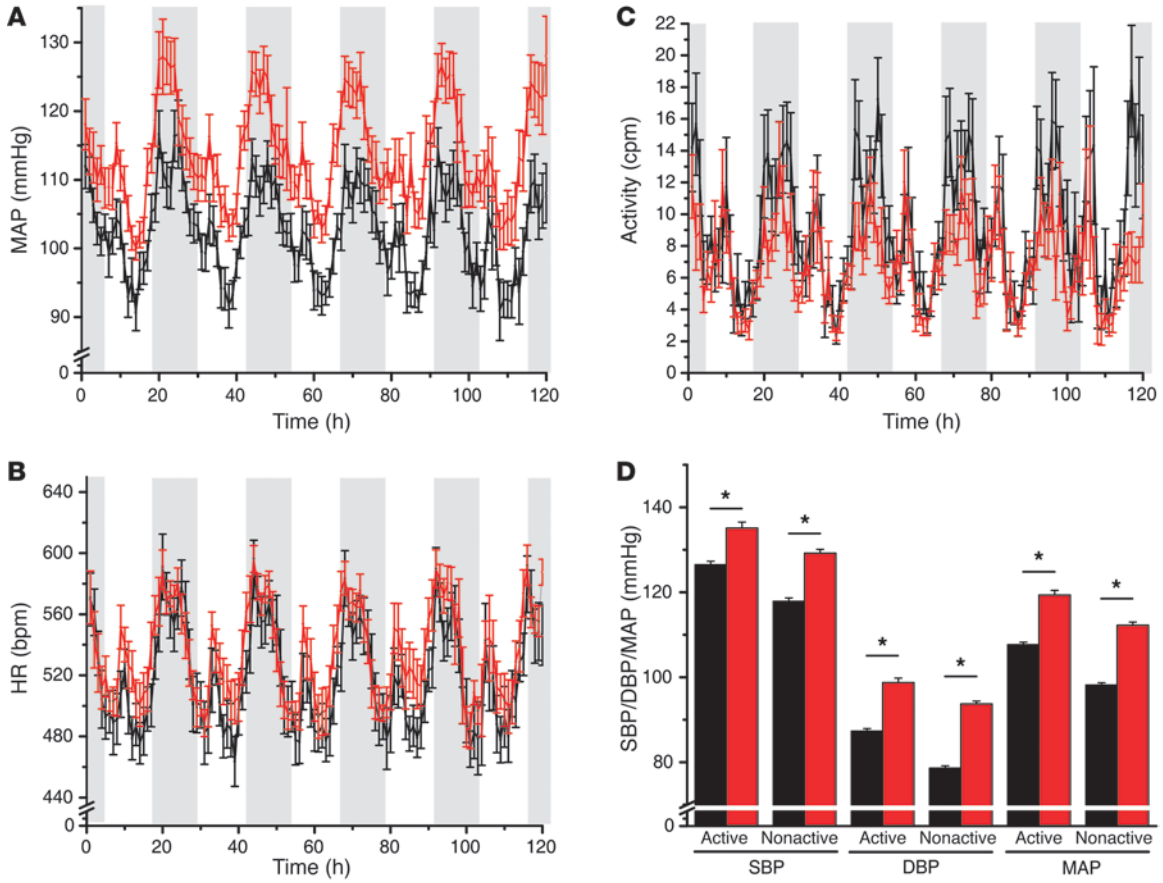

Figure 2

Circadian rhythm of blood pressure, HR, and locomotor activity in TRPM4-deficient mice. Circadian rhythm of MAP (**A**), HR (**B**), and locomotor activity (**C**) of WT (black, $n = 7–13$) and *Trpm4*$^{-/-}$ mice (red, $n = 8–15$) averaged from day 9 to day 13 after implantation of the blood pressure transmitter. The time period between 6:00 p.m. and 6:00 a.m. is marked in gray. (**D**) Activity-dependent analysis of MAP, SBP, and DBP blood pressure from day 9 to day 13 after operation; *$P < 0.01$. Blood pressure values at a locomotor activity score above 9 (active) or below 9 (nonactive) were analyzed.

In this study, we investigated whether TRPM4 is involved in blood pressure regulation using an integrative analysis of participating organ functions. We show that disruption of the *Trpm4* gene in mice increased basal blood pressure without any evidence for impairment of the renin-angiotensin-aldosterone system (RAAS), contractility of peripheral resistance vessels, cardiac function, or body fluid homeostasis. Instead, our data indicate that hypertension in *Trpm4*$^{-/-}$ mice arises from elevated plasma epinephrine levels, likely resulting from increased catecholamine release of chromaffin cells.

Results

Expression of TRPM4 proteins in the cardiovascular system. To identify TRPM4 proteins in cells and tissues of the cardiovascular system, we performed Western blot analysis using protein fractions from WT and *Trpm4*$^{-/-}$ mice and the affinity-purified rabbit polyclonal antibody Ak578 directed against the amino-terminal end of mouse TRPM4 (24). We identified TRPM4 proteins with a size of approximately 138 kDa in aortic endothelial cells, atrium, ventricle, kidney, and adrenal gland of WT mice but not in corresponding tissues or cells of *Trpm4*$^{-/-}$ mice (Figure 1A). This expression pattern suggests that TRPM4 might contribute to blood pressure regulation.

Trpm4$^{-/-}$ *mice are hypertensive.* To characterize cardiovascular functions in TRPM4-deficient mice, we investigated basal hemodynamic parameters by radiotelemetry, which allows simultaneous recording of blood pressure, HR, and physical activity in freely moving mice. After implantation of the pressure transmitters, mice typically show increased blood pressure levels, which slowly decay to a stable baseline after about 1 week (Figure 1B). During that period, which was unchanged in *Trpm4*$^{-/-}$ mice compared with WT, the mice recovered from anesthesia and instrumentation. However, 1 week following the implantation, a steady baseline MAP value could be measured, which was increased by approximately 11 mmHg on average between day 9 and 13 after surgery in *Trpm4*$^{-/-}$ mice (WT: 101.9 ± 0.5 mmHg, $n = 7–13$; *Trpm4*$^{-/-}$: 112.8 ± 0.7 mmHg, $n = 8–15$, $P < 0.001$) (Figure 1, B and E). Both systolic blood pressure (SBP) and diastolic blood pressure (DBP) were significantly increased under these basal conditions in TRPM4-deficient mice, although the largest difference was obvious in DBP (Figure 1, C and E). There was no significant difference in the time course of the heart rate (HR; Figure 1D) and pulse pressure (PP) compared at each single day (data not shown), but when averaged during day 9 until 13 after implantation, HR and PP were slightly increased and decreased, respectively (HR: WT 517.7 ± 1.8 bpm, $n = 7–13$; *Trpm4*$^{-/-}$ 529.9 ± 1.8 bpm, $n = 8–15$, $P < 0.01$; PP: WT 38.9 ± 0.4 mmHg and *Trpm4*$^{-/-}$ 35.4 ± 0.5 mmHg, $P < 0.001$).

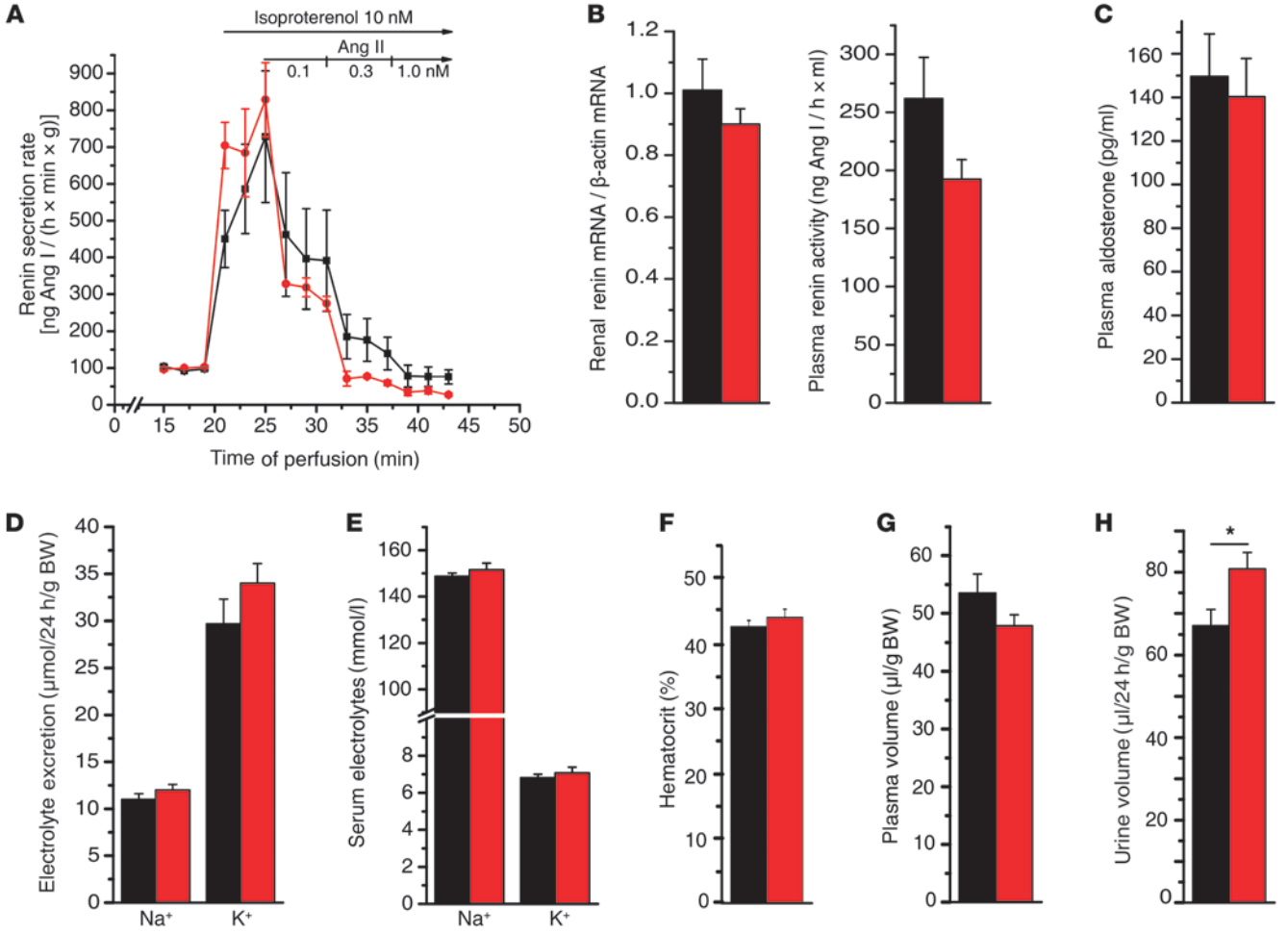

Figure 3

RAAS and fluid balance in *Trpm4*$^{-/-}$ mice. (**A**) Renin secretion rate in the perfusate of isolated kidneys from WT (black) and *Trpm4*$^{-/-}$ (red, $n = 3$ per genotype) mice before and after administration of isoproterenol (10 nM) and Ang II (0.1–1.0 nM). (**B**) Renal renin mRNA expression normalized to β-actin mRNA in WT ($n = 5$) and *Trpm4*$^{-/-}$ mice ($n = 6$) determined via real-time PCR (left panel); and plasma renin activity (right panel) in *Trpm4*$^{-/-}$ ($n = 25$) and WT mice ($n = 23$). (**C**) Plasma aldosterone concentrations in WT and *Trpm4*$^{-/-}$ ($n = 18$ per genotype) mice. (**D**–**H**) Analysis of fluid and electrolyte balance. Electrolyte excretion (WT, $n = 21$; *Trpm4*$^{-/-}$, $n = 22$) in 24-hour urine (**D**), serum electrolyte concentrations ($n = 8$ per genotype, **E**), hematocrit ($n = 8$ per genotype, **F**), plasma volume ($n = 5$ per genotype, **G**), and 24-hour urine volume (WT, $n = 21$; *Trpm4*$^{-/-}$, $n = 22$; $^*P < 0.05$, **H**).

Blood pressure, HR, and physical activity have a circadian pattern characterized by a low period during sleep, a post-awakening rise, and a high plateau period during awake periods. Figure 2, A–C, displays the circadian time course of MAP, HR, and locomotor activity in *Trpm4*$^{-/-}$ and WT mice on days 9 until 13 after implantation of the transmitter. *Trpm4*$^{-/-}$ mice showed an increased MAP during the complete day and night period compared with controls, with acrophases between 6:00 p.m. and 1:00 a.m. HR and locomotor activity were not different between the groups and also showed a clear day/night rhythm. Locomotor activity is an important factor influencing blood pressure (30). Therefore, we analyzed MAP, SBP, and DBP during active versus nonactive phases. The telemetry system produces an activity count that represents a rough index of the animal's locomotor activity. To this end, locomotor activity lower than 9 counts per minute was defined as nonactive conditions and all counts more than 9 as physically active. As shown in Figure 2D, all analyzed pressure parameters were significantly elevated in *Trpm4*$^{-/-}$ mice, and the increase was most pronounced under resting conditions (MAP_{active}: WT 107.7 ± 0.6 mmHg, *Trpm4*$^{-/-}$ 119.3 ± 1.1 mmHg, $P < 0.001$; $MAP_{nonactive}$: WT 98.2 ± 0.5 mmHg, $n = 7$–13, *Trpm4*$^{-/-}$ 112.3 ± 0.7 mmHg, $n = 8$–15, $P < 0.001$). The greatest difference was seen in DBP during nonactive phases ($DBP_{nonactive}$: 78.7 ± 0.6 mmHg in WT, $n = 7$–13; 93.7 ± 0.6 mmHg in *Trpm4*$^{-/-}$ mice, $n = 8$–15, $P < 0.001$). The results indicate that inactivation of TRPM4 leads to a significant shift in arterial blood pressure toward hypertensive levels.

In line with the elevated blood pressure, *Trpm4*$^{-/-}$ mice developed significant, but moderate, cardiac hypertrophy at 6–8 months of age (Supplemental Figure 1A; supplemental material available online with this article; doi:10.1172/JCI41348DS1). Changes in cardiac function can cause alterations in basal blood pressure levels, but pressure-volume measurements in the left ventricle using a miniaturized P-V catheter showed that cardiac output (Supplemental Figure 1B), end systolic elastance, and ejection fraction (data not shown) under basal conditions were not different in

anesthetized *Trpm4*$^{-/-}$ and WT mice. Furthermore, twitch force analysis in electrically stimulated mouse papillary muscle preparations showed no differences in the amplitude of contractions, time to peak, and relaxation time between the genotypes (Supplemental Figure 1, C and D).

Fluid homeostasis and RAAS in Trpm4$^{-/-}$ *mice*. Arterial pressure depends in part on changes in blood volume regulation and total peripheral resistance, which both depend on the RAAS. The capability of renin secretion was analyzed in isolated perfused kidneys. Stimulation of renin secretion with isoproterenol and subsequent inhibition with Ang II were unaltered in the absence of TRPM4 (Figure 3A), excluding an intrinsic defect in renin-producing juxtaglomerular cells. Also, renal expression of renin mRNA was unchanged, and plasma renin activity was not elevated (Figure 3B) but rather decreased, which may be secondary to hypertension. Plasma aldosterone concentrations were not changed between the genotypes (Figure 3C), and analysis of fluid and electrolyte balance showed that excretion of Na^+ and K^+ measured in 24-hour urine samples (Figure 3D) were unaltered, as were serum concentrations of Na^+ and K^+ (Figure 3E). Also, hematocrit (Figure 3F) and plasma volume (Figure 3G) were unaffected. Only urine volume was increased, by approximately 20% (Figure 3H).

Regulation of vascular contractility in Trpm4$^{-/-}$ *mice*. Arterial blood pressure is also determined by interplay of vasoconstrictors and vasodilators and by autoregulatory myogenic mechanisms. For this reason, we studied the reactivity of the vasculature in vivo and in vitro. We tested the effect of TRPM4 deletion on vascular contractility in vivo, in aortic rings, and in perfused resistance vessels. Direct stimulation of α_1-adrenoceptors after i.p. injection of phenylephrine (PE; 1 mg/kg BW) resulted in a comparable rise in MAP and decrease in HR in the two genotypes (Figure 4A). Aortic ring contractility in response to PE was analyzed under isometric conditions in an organ bath, and increasing concentrations of PE did not result in any differences between the genotypes (Figure 4B; EC_{50}: WT 1.0 ± 0.2 μM, n = 7; *Trpm4*$^{-/-}$ 0.9 ± 0.1 μM, n = 8). Likewise, administration of increasing PE concentrations resulted in a comparable reduction in flow and rise in vascular resistance in the isolated perfused hind limbs of *Trpm4*$^{-/-}$ and WT mice (Figure 4, C and D). The absolute values for baseline flow were also unchanged (WT: 11.0 ± 1.1 ml/min, *Trpm4*$^{-/-}$: 13.3 ± 0.9 ml/min, n = 9 per genotype), and with the highest dose of PE (bolus of 100 μM), perfusate flow was severely reduced (WT: 1.5 ± 0.4 ml/min, *Trpm4*$^{-/-}$: 2.1 ± 0.4 ml/min, n = 9 per genotype). In addition, administration of epinephrine, a nonselective adrenoceptor agonist, resulted in similar changes in flow. At lower concentrations, an increase in perfusion flow consistent with β-adrenoceptor stimulation was observed in both groups, and with increasing epinephrine concentrations, vasoconstriction mediated through activation of α-adrenoceptors became more apparent (Figure 4E). β-Adrenoceptor stimulation with isoproterenol in vivo (2 μg/kg i.p.) did not reveal any difference in HR response (Supplemental Figure 2A) or blood pressure (data not shown), and there was also no difference in relaxation of smooth muscle cells in peripheral resistance vessels (Supplemental Figure 2B).

The arterial endothelium modulates vascular contractility and thus blood pressure by releasing vasoactive substances, and in many models of hypertension high blood pressure is associated with impaired endothelium-dependent vasorelaxation (31). Endothelium-dependent relaxation following acetylcholine application was tested in aortic rings (data not shown) as well as in isolated perfused hind limb experiments (Figure 4F) but was not altered in *Trpm4*$^{-/-}$ mice. In addition, the contribution of nitric oxide release to the maintenance of resting blood pressure was tested by injection of the nitric oxide synthase inhibitor *N*ω-nitro-L-arginine methyl ester (L-NAME; 25 mg/kg i.p.). The resulting increase in blood pressure and reflectory bradycardia were comparable in WT and *Trpm4*$^{-/-}$ mice (Supplemental Figure 2, C and D), indicating that TRPM4 does not represent a critical determinant of nitric oxide formation in resistance vessels in vivo.

To test whether TRPM4 is involved in the regulation of myogenic response in resistance vessels, we investigated pressure-dependent changes in vascular resistance of the hind limbs of WT and TRPM4-deficient mice. For all experiments, perfusion pressure was gradually increased to 100 mmHg; at this perfusion pressure, spontaneous myogenic tone developed in the vasculature, as verified by application of vasodilating substances such as acetylcholine (Figure 4F). To study myogenic response, 10 mmHg incremental pressure steps starting from 50 mmHg to 120 mmHg were applied; thereafter, the same protocol was applied using calcium-free perfusate to calculate the active response at defined transmural pressures. Elevation of intravascular pressure induced a similar increase in vascular resistance in *Trpm4*$^{-/-}$ and WT mice (Figure 4, G and H), demonstrating that elevated blood pressure cannot be explained by impaired myogenic responses of peripheral small arteries and arterioles, which is inherent to smooth muscle (32).

Ang II formed by Ang I–converting enzyme (ACE) is one of the most important vasoconstrictors in regulating blood pressure. However, blood pressure is also regulated by ACE-independent Ang II generation, which is mediated by chymases, serine proteases primarily secreted from mast cells residing in the interstitial compartment of blood vessels (33, 34). Mast cell degranulation is enhanced in *Trpm4*$^{-/-}$ mice (24). To rule out an increased mast cell–derived chymase activity in the generation of hypertension in *Trpm4*$^{-/-}$ mice, we analyzed chymase-catalyzed Ang II formation and subsequent contraction of resistance vessels following application of the Ang I analog [Pro^{11},$DAla^{12}$]Ang I, a substrate for Ang II generation by chymase, but not by ACE. Application of a perfusate containing 1 μM [Pro^{11},$DAla^{12}$]Ang I resulted in a 46% reduction in perfusate flow within 60 seconds in WT vessels and a comparable decrease in perfusion flow and increase in vascular resistance in the hind limb vasculature of *Trpm4*$^{-/-}$ mice (Supplementary Figure 2, E and F).

Neurogenic mechanisms contribute to hypertension in Trpm4$^{-/-}$ *mice*. Influences by the CNS on blood pressure regulation may be mediated by changes in the adjustment of the tone in the parasympathetic and sympathetic nervous system, and inappropriately high sympathetic activity is commonly observed in patients with essential hypertension (35, 36). Due to expression of TRPM4 in the adrenal gland (Figure 1A) and in several regions of the CNS including thalamus, hypothalamus, medulla oblongata, pons, and spinal cord (37), we tested an involvement of neurogenic mechanisms in the development of hypertension in *Trpm4*$^{-/-}$ mice. We inhibited ganglionic transmission with the nicotinic acetylcholine receptor blocker hexamethonium (20 mg/kg i.p.). When the sympathetic as well as the parasympathetic influence was blocked, TRPM4-deficient mice showed a larger reduction in blood pressure, so that the difference in basal MAP levels between the genotypes was abolished (Figure 5, A and B). Likewise, the difference in MAP was also abolished after α_1-adrenergic blockade by prazosin (Figure 5C). This suggests

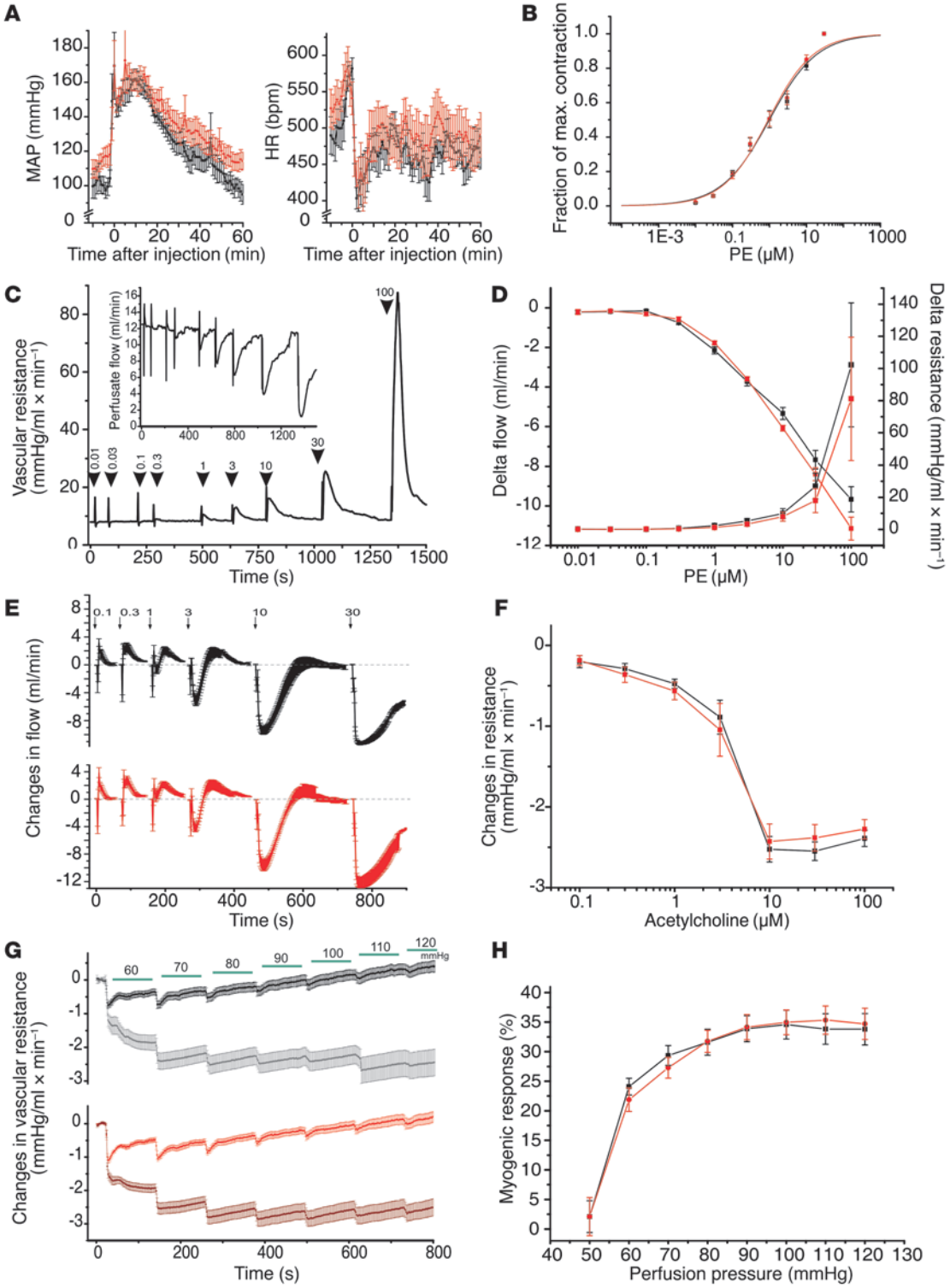

Figure 4

Vascular reactivity in *Trpm4*$^{-/-}$ mice. (**A**) MAP and HR after i.p. injection (at time point 0 minutes) of PE (1.0 mg/kg BW; WT, black, $n = 7$; *Trpm4*$^{-/-}$ red, $n = 9$). (**B**) Concentration-response curve of PE-induced contraction of isolated aortic rings (WT $n = 7$, *Trpm4*$^{-/-}$ $n = 8$). (**C**) Time course of vascular resistance of the vasculature of isolated hind limbs calculated from perfusion pressure and perfusate flow (inset); bolus injections (200 μl) of increasing PE concentrations (in μM) are indicated by arrowheads. (**D**) Dose-response curves of changes in flow and vascular resistance after application of PE in the perfused hind limb vasculature ($n = 9$ per genotype). (**E**) Averaged changes in perfusate flow after bolus injections (200 μl) of increasing epinephrine concentrations (in μM; $n = 6$ per genotype). (**F**) Changes in vascular resistance of the perfused hind limb after bolus injections (200 μl) of increasing acetylcholine concentrations ($n = 7$ per genotype). (**G** and **H**) Analysis of pressure-induced vascular resistance. Average change in vascular resistance (**G**) using physiological KH solution (black, red) or Ca^{2+}-free KH (gray, dark red) as perfusate in WT (upper panel, $n = 11$) or *Trpm4*$^{-/-}$ mice (lower panel, $n = 10$); intravascular pressure is indicated. (**H**) Analysis of the myogenic response in dependence of the intravascular pressure calculated from measurement in **G**.

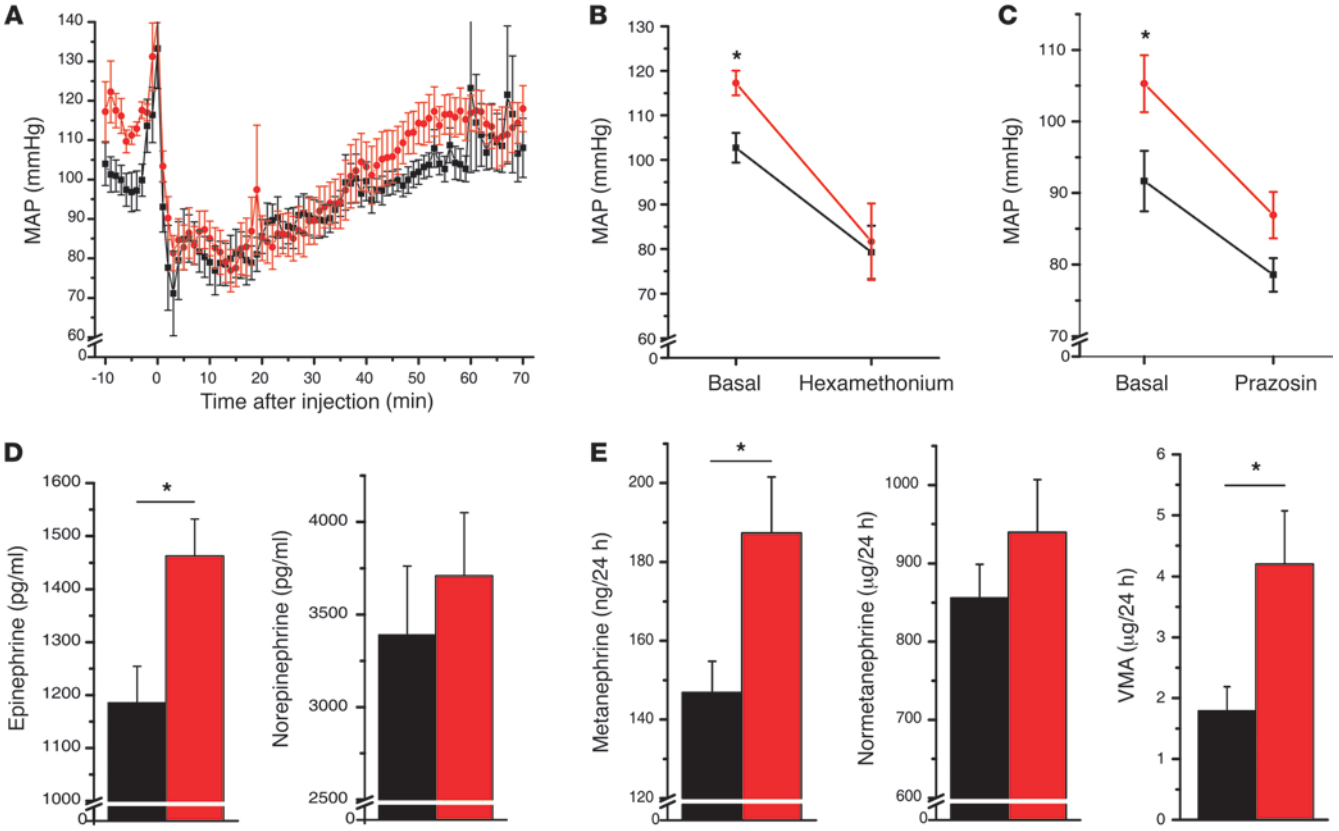

Figure 5

Neurogenic mechanisms contribute to hypertension in *Trpm4*$^{-/-}$ mice. (**A**) Time course of MAP before and after inhibition of ganglionic transmission by hexamethonium (20 mg/kg i.p.) in *Trpm4*$^{-/-}$ (red, $n = 9$) and WT (black, $n = 7$) mice. (**B** and **C**) Averaged peak response of MAP to injection of hexamethonium (*$P < 0.01$) (**B**) or prazosin (1 mg/kg i.p.; WT, $n = 7$, *Trpm4*$^{-/-}$, $n = 9$; *$P < 0.05$, **C**). (**D**) Plasma epinephrine and norepinephrine concentrations in WT and *Trpm4*$^{-/-}$ mice ($n = 14$ per genotype, *$P < 0.01$). (**E**) Catecholamine metabolite concentration in urine collected for 24 hours from WT ($n = 15$; for VMA, $n = 6$) and *Trpm4*$^{-/-}$ mice ($n = 14$; for VMA, $n = 8$; *$P < 0.05$).

that the TRPM4-deficient mice may exhibit an increased sympathetic tone. As elevated sympathetic nerve activity often results in increased systemic catecholamine levels, plasma epinephrine and norepinephrine level, as well as levels of their urinary metabolites metanephrine, normetanephrine, and vanillyl mandelic acid (VMA) were determined. Strikingly, plasma epinephrine levels and urinary excretion of metanephrine and VMA were found to be significantly elevated in TRPM4-deficient mice in comparison to WT mice (Figure 5, D and E).

TRPM4 regulates catecholamine release of chromaffin cells. To rule out that the higher plasma epinephrine level in *Trpm4*$^{-/-}$ mice is due to the presence of adrenal gland tumors (pheochromocytomas), we analyzed adrenal glands from WT and TRPM4-deficient mice histologically. Macroscopically, the adrenal glands were of the same size in both genotypes. Microscopic examination of H&E-stained sections revealed no abnormalities in structure or size of cortex and medulla. Also, there were no signs of chromaffin cell hyperplasia or increased numbers of mitotic figures (Figure 6A). Since pheochromocytomas occur in conditions with specific types of multiple endocrine neoplasia (MEN) syndromes, which also include tumors of several endocrine glands, we wanted to exclude a MEN-like-phenotype and analyzed different tissues affected in MEN but could not find any obvious differences in *Trpm4*$^{-/-}$ compared with WT organs (Supplemental Figure 3). In order to confirm expression of TRPM4 in chromaffin cells, we used laser capture microdissection to isolate cell clusters from adrenal medullae, which indeed expressed Trpm4 cDNA (Figure 6B). To characterize the possible role of TRPM4 in catecholamine release from individual dissociated chromaffin cells, we applied carbon fiber amperometry and simultaneous microfluorimetric measurements of cytosolic calcium concentration using Fura-2 (Figure 6C). Application of the physiological transmitter acetylcholine (10 μM) resulted in a fast rise in intracellular calcium concentration followed by a slow decay toward a plateau level (Figure 6C). Calcium concentrations at baseline and at different time points during acetylcholine stimulation were comparable in WT and *Trpm4*$^{-/-}$ mice (Figure 6D). Spontaneous amperometric events measured in parallel were not different under basal conditions (Figure 6E), but in contrast, *Trpm4*$^{-/-}$ chromaffin cells showed a significantly larger number of spikes after stimulation with acetylcholine (Figure 6F). Since morphological alterations could contribute to changes in neurotransmitter secretion in *Trpm4*$^{-/-}$ chromaffin cells, we also analyzed the chromaffin cell ultrastructure in both genotypes. Ultrathin sections from adrenals were examined using electron microscopy (Supplemental Figure 4A). Individual

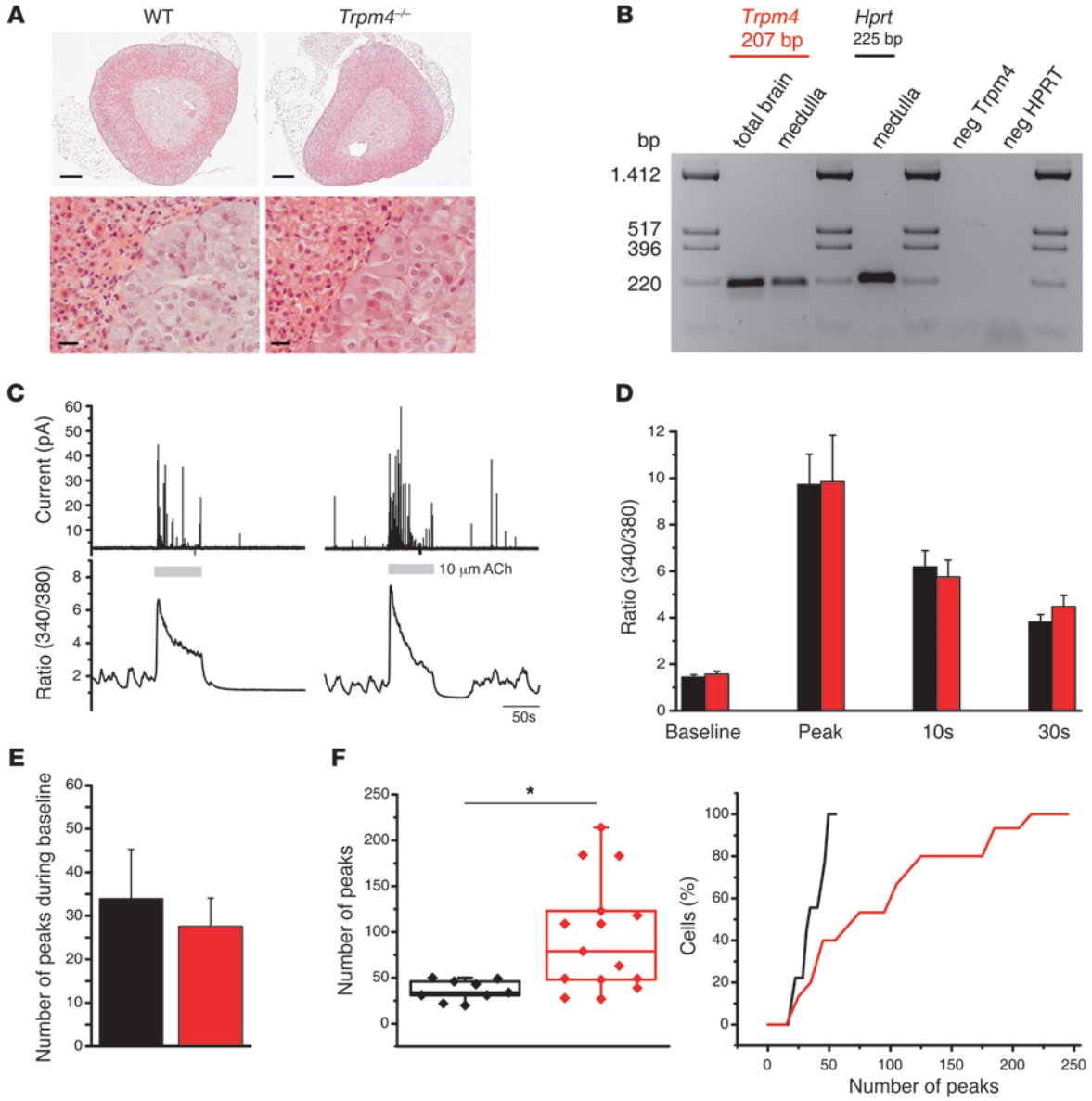

Figure 6

Adrenal gland phenotype in *Trpm4*$^{-/-}$ mice. Increased rate of acetylcholine-induced catecholamine release from TRPM4-deficient chromaffin cells. (**A**) Representative examples of H&E-stained adrenal gland sections from WT and *Trpm4*$^{-/-}$ mice. Scale bars: 100 μm (upper panels) and 20 μm (lower panels). (**B**) Amplification of *Trpm4* and *Hprt* transcripts by RT-PCR from RNA of cell clusters dissected from the adrenal medulla. neg Trpm4 and neg HPRT indicate amplifications without template cDNA. (**C**) Representative traces of carbon fiber amperometry and simultaneous measurements of intracellular calcium concentration ($[Ca^{2+}]_{cyt}$) in chromaffin cells from WT and *Trpm4*$^{-/-}$ mice. (**D**) Averaged $[Ca^{2+}]_{cyt}$ before (baseline) and at indicated time points after application of acetylcholine (ACh; 10 μM) in chromaffin cells from WT (n = 9) and *Trpm4*$^{-/-}$ mice (n = 14). (**E**) Number of amperometric events under basal conditions during 5 minutes before stimulation in WT (n = 9) and *Trpm4*$^{-/-}$ (n = 14) chromaffin cells. (**F**) Box plot (left) and cumulative analysis (right) of amperometric events after stimulation with 10 μM acetylcholine in WT (n = 9) and *Trpm4*$^{-/-}$ (n = 14) chromaffin cells. *P < 0.01; WT and *Trpm4*$^{-/-}$ values in the cumulative probability plot are significantly different (Kolmogorov-Smirnov test, P = 0.015).

cells appeared to have a collection of smaller vesicles and a second group of larger vesicles, as described previously (38), but we could not detect any difference in the relative frequency distribution of vesicle size between WT and *Trpm4*$^{-/-}$ chromaffin cells. Also, the total area of all vesicles relative to the total cell area as a correlate for catecholamine content of the chromaffin cells was unaltered between the genotypes (Supplemental Figure 4B).

Discussion

TRPM4 proteins act as calcium-activated nonselective cation channels in mast cells that critically limit the driving force for calcium influx, release of inflammatory mediators, and anaphylactic responses (24). Here we identify TRPM4 proteins in endothelial cells, atrium, ventricle, kidney, and adrenal gland of WT mice but not in corresponding tissues or cells of *Trpm4*$^{-/-}$

mice. We demonstrate that inactivation of TRPM4 significantly alters long-term regulation of blood pressure, with a significant resetting toward hypertensive levels. Using an integrative analysis of the major organ functions involved in blood pressure regulation, we provide comprehensive evidence that neurogenic mechanisms contribute to blood pressure elevation in *Trpm4*$^{-/-}$ mice and that alterations in the RAAS including the mast cell–mediated chymase activity, cardiac output, contractility of papillary muscle, contractility of peripheral resistance vessels, electrolyte or fluid balance, as well as locomotor activity are unlikely as main pathogenic factors.

Telemetric long-term blood pressure measurements in conscious and freely moving mice facilitate an accurate direct assessment of arterial pressure that is not confounded by the stress of tethering or a limited number of sampling times. Using this method, we show that *Trpm4*$^{-/-}$ mice exhibit significant elevation of 24-hour average SBP, DBP, and MAP of 9 mmHg, 12 mmHg, and 11 mmHg, respectively. This blood pressure elevation is preserved throughout the complete diurnal rhythm. The radiotelemetry system has the ability to dissect indirect influences on hemodynamic variables that may arise as a consequence of behavioral changes. This is of particular importance, since an increase in activity and subsequently in HR directly correlates with blood pressure elevation in mice (30). In *Trpm4*$^{-/-}$ mice, the circadian rhythm of locomotor activity is unaltered. Thus, an activity-driven hypertension in *Trpm4*$^{-/-}$ mice can be excluded, especially since the analysis of blood pressure levels at physical rest revealed an even more pronounced elevation of SBP, DBP, and MAP of 11 mmHg, 15 mmHg, and 14 mmHg, respectively, compared with WT controls.

In order to approach the mechanism by which deletion of TRPM4 leads to resetting of long-term blood pressure regulation, we tested the major organ functions involved in blood pressure regulation. TRPM4 is expressed in several cell types of the heart, including cells of the sinoatrial node (27), and Purkinje fibers (28). Recently, a mutation in exon 1 of the human *TRPM4* gene was identified in patients with progressive familial heart block type I (PFHBI) leading to substitution of glutamic acid at position 7 by lysine (TRPM4^{E7K}), resulting, apparently, in a gain-of-function phenotype (28). In *Trpm4*$^{-/-}$ mice, HR under resting conditions, physical activity, and isoproterenol stimulation were unchanged, but a detailed analysis of cardiac conductivity was not performed in our study. Blood pressure elevation in *Trpm4*$^{-/-}$ mice was associated with moderate cardiac hypertrophy. TRPM4 channel activity is upregulated in cardiomyocytes from hypertrophied hearts (29). However, contractility of isolated papillary muscles as well as basal cardiac output in anesthetized mice was comparable in WT and *Trpm4*$^{-/-}$ mice. These data suggest that hypertension in *Trpm4*$^{-/-}$ mice is likely not due to altered cardiac performance.

Next we tested the possibility of an impaired function of the kidney and the RAAS. Renin secretion is under tight control of NaCl sensing in macula densa cells, where TRPM4-like channels were described (39). However, we did not detect any difference in the regulation of renin secretion in isolated kidneys, renal renin expression, plasma renin concentration, and aldosterone levels. Therefore, we rule out an intrinsic defect in renin secretion from juxtaglomerular cells, and impaired negative feedback regulation by macula densa cells on renin secretion from juxtaglomerular cells also seems to be unlikely. In addition, excretion of Na^+ and K^+, serum concentrations of Na^+ and K^+, hematocrit, and plasma volume were unaffected in *Trpm4*$^{-/-}$ mice. Only urine volume was increased, by approximately 20%, which may have been due to pressure diuresis. Together, these results argue against chronic volume retention as the main pathogenic factor in the maintenance of arterial hypertension in *Trpm4*$^{-/-}$ mice.

MAP is determined by cardiac output and total peripheral resistance. In the light of elevated SBP, DBP, and MAP, a slight decrease in PP, and no alterations in cardiac output, we hypothesized that peripheral resistance could be increased. Pressure-induced vasoconstriction of small arteries and arterioles is a major component in the control of vascular resistance and, thus, blood pressure (32). Recently, a role of TRPM4 as mechanosensor mediating myogenic vasoconstriction was reported in cerebral arteries (26). However, a role of TRP channels in generating myogenic tone was recently challenged (40). We analyzed pressure-induced vasoconstriction in peripheral resistance vessels of perfused hind limbs. This myogenic response of the resistance vessels is inherent to smooth muscle and independent of neural, metabolic, and hormonal influences. However, we could not find any difference in pressure-induced myogenic response in the hind limb vasculature of *Trpm4*$^{-/-}$ mice in comparison to controls, demonstrating that elevated blood pressure cannot be explained by impaired myogenic response of peripheral small arteries and arterioles. Although these results initially seem to be contradictory to the findings of Earley et al. (10), this may be well due to differences in the characteristics of the investigated type of blood vessels. The role of myogenic tone for blood flow regulation is probably more relevant in the kidney and the brain than in other organ systems, and in comparison to hind limb arterioles cerebral arteries may exhibit specific mechanisms to prevent large changes in cerebral blood flow, which may result in hypoxia or overperfusion of the brain. Therefore, the relevant mechanosensors regulating myogenic response may differ between these vessel types.

Arterial blood pressure is determined not only by autoregulatory myogenic mechanisms but also by interplay of vasoconstrictors and vasodilators. However, smooth muscle–dependent vasoconstriction of peripheral resistance vessels induced by stimulation of α_1-adrenoceptors, β-adrenoceptor–mediated vasodilation, and endothelium-dependent vasodilation was unchanged in *Trpm4*$^{-/-}$ mice. Also, vasoconstriction induced by ACE-independent Ang II formation by mast cell–derived chymase was not different in *Trpm4*$^{-/-}$ mice. It was important to rule out an increase in chymase activity in TRPM4-deficient vessels, since we recently showed that inactivation of TRPM4 leads to enhanced mast cell degranulation (24).

An increase in blood pressure should lead to baroreflex inhibition of sympathetic activity. In such a case, the sympathetic inhibition should reduce HR and catecholamine release from nerve endings and chromaffin cells. In contrast, we found in *Trpm4*$^{-/-}$ mice a slight increase in HR, elevated epinephrine levels in plasma, as well as elevated urinary excretion of metanephrine and VMA. Norepinephrine and normetanephrine levels were also higher on average, but this was not statistically significant. This may be explained by the distinct sources of the circulating catecholamines epinephrine and norepinephrine. Epinephrine is released by the chromaffin cells in the adrenal medulla upon activation of preganglionic sympathetic nerves innervating this tissue. Norepinephrine is also released by the adrenal medulla but represents only approximately 20% of its total catecholamine release, and the primary source of circulating norepinephrine is spillover from sympathetic nerves. In addition to showing elevated plasma epinephrine levels, *Trpm4*$^{-/-}$ mice had increased MAP that decreased to the WT level upon injection of hexamethonium, an inhibitor of ganglionic transmis-

sion of both the sympathetic and parasympathetic nerves. Also, prazosin, which primarily blocks vasoconstriction induced by α_1-adrenergic receptors, decreased blood pressure more strongly in *Trpm4*$^{-/-}$ than in control mice.

Together, these results suggest that the TRPM4-deficient mice have increased sympathetic tone. The more pronounced increase in epinephrine versus norepinephrine plasma levels and the reversal of elevated blood pressure by the ganglionic blocker hexamethonium may point to a major role of TRPM4 in the regulation of either the catecholamine release from chromaffin cells of the adrenal medulla or in the regulation of the activity of preganglionic sympathetic nerves innervating this tissue. Adrenal glands from mice of both genotypes did not exhibit histological abnormalities, such as pheochromocytoma, and these mice did not show any signs or symptoms of multiple endocrine neoplasia. In contrast, genetic deletion of TRPM4 led to an increased number of exocytotic events in chromaffin cells from adrenal medulla after stimulation with the physiological neurotransmitter acetylcholine. This increase was not associated with changes in intracellular calcium signaling. Since there were no changes in relative frequency distribution of dense core vesicle diameter and relative cellular vesicle content, alterations in the biogenesis of chromaffin vesicles are unlikely to be a reason for the higher number of exocytotic events. Thus, our results indicate that TRPM4 serves as a negative regulator of exocytotic catecholamine release, at least in chromaffin cells. Possibly, catecholamine release is also regulated in the same direction in other neurons of the sympathetic nervous system. The molecular mechanism underlying how TRPM4 regulates or contributes to chromaffin cell release still needs to be clarified but may include a direct TRPM4-dependent regulation of vesicle release, as has been shown for another TRPM, TRPM7, in cholinergic synaptic vesicles (41).

In summary, we have found that inactivation of the *Trpm4* gene induces hypertension in mice. Our systematic analysis of the underlying mechanisms indicates that increased catecholamine secretion from adrenal chromaffin cells and sympathetic overdrive significantly contributes to elevated blood pressure in TRPM4-deficient mice. These results suggest that TRPM4 activity might be beneficial not only for preventing allergic reactions as proposed before but may also limit blood pressure increase in hypertensive patients.

Methods

Animals. The generation of *Trpm4*$^{-/-}$ mice used in this study was previously described (24). Experiments were performed on 3 -to 8-month-old male 129/SvJ and TRPM4-deficient mice that were backcrossed for at least 6 generations into the 129/SvJ background. Mice were housed in an essentially specific pathogen–free environment with a 12-hour light/12-hour dark cycle and allowed water and standard food (0.24% sodium, ssniff Spezialdiäten) ad libitum. All animal experiments were performed according to the NIH *Guide for the Care and Use of Laboratory Animals* (publication no. 85-23. Revised 1985) and were approved by the local ethics committee.

Telemetric blood pressure measurements. We used a radiotelemetry system (PA-C10, Data Science International) to monitor blood pressure in conscious, unrestrained mice, as described previously (42). Briefly, we implanted the pressure-sensing catheter into the left carotid artery and inserted the transducer unit into a subcutaneous pouch along the right flank. During and after a recovery period of at least 1 week, we collected, stored, and analyzed arterial pressure recordings with Dataquest A.R.T. software 3.0. We collected data for basal blood pressure with a 10-second scheduled sampling every 3 minutes, and 24-hour mean values for MAP, SBP, DBP, PP, and HR were calculated. To analyze the acute effects of different substances, we collected data continuously in 5-second intervals and averaged blood pressure values over an interval of 1 minute. The following drugs were applied: prazosin (1 mg/kg BW), PE (0.1, 0.3, and 1 mg/kg BW), hexamethonium (20 mg/kg BW), isoproterenol (2 μg/kg BW), and L-NAME (25 mg/kg BW).

Isolated perfused hind limb. The abdominal aorta was prepared during avertin (Sigma-Aldrich, 0.6 mg/g BW) anesthesia; a cannula (Hugo Sachs) was introduced caudal to the renal arteries and tied with a 7/0 suture. The inferior caval vein was slit open longitudinally to prevent venous congestion. A roller pump was used to perfuse the hind limb with filtered Krebs-Henseleit (KH) solution of the following composition (mmol/l): 118 NaCl, 4.7 KCl, 2.52 $CaCl_2$, 1.64 $MgSO_4$, 24.88 $NaHCO_3$, 1.18 KH_2PO_4, 5 glucose, 1 sodium pyruvate. The perfusion pressure was regulated using a manometer. Perfusion started with a pressure of 70–80 mmHg that was gradually increased to 100 mmHg. At this perfusion pressure, a considerable amount of spontaneous myogenic tone is present, which makes preconstriction unnecessary. When a stable baseline was reached, PE, epinephrine, isoproterenol, or acetylcholine was applied as a bolus (200 μl) in KH solution. The Ang I analog [Pro^{11},DAla^{12}]Ang I was perfused as a 1-μM solution over 1 minute. Vascular resistance was calculated as perfusion pressure divided by flow rate.

For measuring the spontaneous myogenic tone, the vascular bed was subjected to a series of pressure steps between 50 and 120 mmHg. After completion of the pressure response curve in KH solution, perfusion pressure was gradually restored to 50 mmHg, and perfusion with Ca^{2+}-free KH solution was started. The pressure response curve was repeated under these conditions to obtain passive responses. At each pressure step, myogenic tone of the hind limb vascular bed was calculated as the difference between the resistance with and without calcium divided by the resistance with calcium (32).

Determination of cardiac hypertrophy, hematocrit, and electrolytes. Cardiac hypertrophy index was analyzed in mice between 6 and 8 months of age. Hematocrit was measured by collection of a drop of blood into a hematocrit capillary via submandibular puncture and spinning it in a microfuge (Hettich). Blood samples for electrolyte determination were taken via submandibular puncture into tubes and centrifuged to obtain serum. For determination of urinary electrolytes, mice were housed in individual metabolic cages (Hatteras Instruments) and urine was collected for 24 hours with free access to water and chow. Urine and serum concentrations of sodium and potassium were measured by standard flame photometry (Eppendorf).

Determination of plasma volume. Plasma volume was determined with the Evan's blue dilution method (43). Mice were anesthetized with isoflurane, and 30 μl of an Evan's blue stock solution (Sigma-Aldrich, 0.5% w/v in sterile isotonic saline) was injected intravenously into the tail vein. Five minutes later, blood was collected via submandibular puncture for determination of circulating Evan's blue levels, and the mice were sacrificed. The plasma samples (10 μl) were diluted in 190 μl saline, and dye concentration was read at 605 nm on a spectrophotometer (Infinite 200, Tecan Group Ltd.). Dye dilution was calculated by extrapolation from an Evan's blue standard curve prepared in mouse plasma and is expressed in microliters per gram body weight.

Determination of plasma catecholamines and their urinary metabolites. Catecholamines and their metabolites were determined by HPLC with electrochemical detection (ECD). Epinephrine and norepinephrine in plasma were determined as described previously (44). To avoid the possible interference with the results, extreme care was taken when collecting the samples to keep the sampling circumstances similar for all animals. Blood samples were taken by submandibular bleeding within 10 seconds of capture of the mouse. Urine was collected for 24 hours in metabolic cages. Acidified urine was analyzed by HPLC with ECD using commercially available kits for VMA (ClinRep Diagnostic Kit for VMA in Urine, Recipe Chemicals and Instruments) and for metanephrine and normetanephrine (Bio-Rad).

In vitro studies on isolated aortic rings. The thoracic aortas were dissected free, and the adhering fat and connective tissue were removed carefully. The arteries were placed in KH solution (see *Isolated perfused hind limb*). Rings (2–3 mm long) were suspended in an organ bath (FMI GmbH) using steel wires for recording isometric contractile force (PowerLab, ADInstruments). The organ chambers were filled with warmed (37°C), aerated (95% O_2, 5% CO_2) KH solution. The rings were allowed to equilibrate for 1 hour at their optimal resting tension of 1 g. After stabilization, they were exposed 3 times to 40 mmol/l KCl before the generation of concentration response curves with receptor agonists.

Measurement of cardiac output and contractility of papillary muscles. Cardiac output was measured using a 1.4 F high-fidelity pressure conductance catheter (Millar Instruments Inc.) in anesthetized mice (1.2 g/kg urethane; 50 mg/kg α-chloralose). They were intubated and ventilated with room air using a positive ventilation pressure. After exposure of the right carotid artery, the catheter was introduced and forwarded into the left ventricle. After hemodynamic stabilization, baseline P-V loops were recorded. Decreased left ventricular preload was obtained by temporary occlusion of the inferior vena cava.

For papillary muscle isolation, hearts of the mice were quickly removed and transferred to a dissection chamber containing KH solution with 30 mM 2,3-butanedione monoxime (BDM) gassed with 100% O_2. With the help of a stereoscopic microscope, the anterior papillary muscle of the left ventricle was dissected together with part of valvular sail and ventricular wall to attach fine sutures without damaging the muscle. The papillary muscles were fixed vertically in the organ bath containing KH solution (1.5 mM $CaCl_2$), continuously gassed with carbogen, and maintained at 32°C. Field stimulation was provided by isolated rectangular pulses (2-ms duration at 1 Hz) applied through a pair of platinum electrodes. The stimulation started immediately after transfer of the preparation in the organ bath, and the muscles were gradually stretched to nearly maximal twitch force and allowed to equilibrate for 45–60 minutes. Time to peak tension and time to 50% relaxation was calculated using Chart 5.5 software (ADInstruments).

Isolated perfused kidney model. Kidneys of WT and *Trpm4*$^{-/-}$ mice were perfused as described in Schweda et al. (45). Briefly, the abdominal aorta was cannulated, and the right kidney was excised, placed in a thermostated moistening chamber, and perfused at constant pressure. The renal vein was cannulated, and the venous effluent was collected for determination of renin activity and venous blood flow. The basic perfusion medium consisted of a modified KH solution supplemented with 6 g/100 ml bovine serum albumin and with freshly washed human red blood cells.

Determination of plasma aldosterone, plasma renin concentration, and renal renin expression. Plasma aldosterone concentrations were quantified as duplicates with an ELISA (DRG Instruments GmbH) according to the manufacturer's protocol. For determination of plasma renin concentration, the blood samples taken by submandibular bleeding were centrifuged, and the plasma was incubated for 1.5 hours at 37°C with plasma from bilaterally nephrectomized male rats as renin substrate. The generated Ang I (ng/ml × h) was determined by radioimmunoassay (Byk & DiaSorin Diagnostics). After isolation of total RNA from the kidney, renin and cytosolic β-actin were measured by quantitative RT-PCR (46). The signal was related to those obtained for β-actin mRNA.

Western blot analysis. For Western blots, a rabbit polyclonal antibody (Ak578) directed against the aminoterminal end of mouse TRPM4 was generated and affinity purified (24). Specificity of antibodies was confirmed using comparative analysis of protein fractions from WT and *Trpm4*$^{-/-}$ mice. Antibodies for calnexin (Abcam plc), $Ca_V\beta_2$ (47), and synaptophysin (Synaptic Systems GmbH) served as controls for protein loading.

Reagents and chemicals. Phenylephrine, isoproterenol, prazosin, hexamethonium, and L-NAME were purchased from Sigma-Aldrich. The Ang I analog [Pro^{11},DAla^{12}]Ang I was purchased from Bachem California Inc.

Histology. Three mice of each genotype were cardially perfused with PBS and fixed with PBS containing 4% PFA. Organs were dissected separately, except trachea, thyroid, parathyroid, and esophagus, which were dissected en bloc. All tissues were processed and embedded in paraffin wax. Serial sections were cut to a thickness of 5 μm for pituitary and pancreas and 10 μm for the thyroid trachea block and documented using a Zeiss microscope (Axio Observer A.1).

Laser capture microdissection. A PALM Laser Microdissection System with autocatapult and Robocut software (Zeiss) was used for microdissection. Frozen-tissue specimens were cut at 8–9 μm thickness and serial sections transferred to PALM Membrane Slides (Zeiss).Tissue cryosections were fixed with ethanol and stained with cresyl violet. Stained slices were kept in ethanol at 4°C until microdissection (30 minutes to 8 hours). Approximately 15 minutes before microdissection, individual slides were air-dried at room temperature. Clusters of chromaffin cells were microdissected and catapulted into sterile oil-covered caps of 0.5 ml tubes. Per cap, approximately 15–25 chippings were collected per tube. For RNA isolation, chippings were dissolved in buffer RLT (QIAGEN) after microdissection and snap frozen on dry ice. Total RNA was extracted from individual caps using the QIAGEN RNeasy Micro Kit employing DNase on column digestion. Eluted RNA was used for one-step RT-PCR (Invitrogen).

The following intron-spanning primers were used for amplification of *Trpm4* fragments: IN48 (5′-TCTTCACACTGCGCCTGCTG-3′) and IN49 (5′-GTCGGTAGAAGACCCTGCGC-3′), resulting in a 207-bp fragment. *Hprt* fragments were amplified as a positive control: UW637 (5′-GCTCGAGATGTCATGAAGG-3′) and UW638 (5′-AGTTGAGAGATCATCTCCACC-3′), resulting in a 225-bp fragment. Also, as positive control, total RNA from complete brain was used as template.

Preparation of mouse chromaffin cells. Following cervical dislocation, adrenal glands were dissected and placed in filtered Locke's solution (154 mM NaCl, 5.6 mM KCl, 3.6 mM $NaHCO_3$, 5 mM HEPES, 5.6 mM glucose, pH 7.3). The cortex was removed, and the medullae were digested using papain-containing medium (250 ml DMEM medium supplemented with 50 mg L-cysteine, 2.5 ml 0.1 M $CaCl_2$, 2.5 ml 50 mM EDTA, and 20–25 U/ml papain [Worthington]) at 37°C for 40 minutes with slight shaking, followed by addition of an inhibitor solution (225 ml DMEM supplemented with 25 ml heat-inactivated fetal calf serum [Invitrogen], 625 mg albumin, 625 mg trypsin inhibitor [Sigma-Aldrich]) for 5–10 minutes to stop digestion. Subsequently, the tissue was triturated gently, and the cell suspension was transferred into another tube with fresh enriched DMEM (500 ml DMEM supplemented with 2 ml penicillin/streptomycin and 5 ml insulin-transferrin-selenium-X [Invitrogen]), triturated again, and centrifuged 5 minutes at 80 *g* and 37°C. The supernatant was removed and the pellet gently resuspended in enriched DMEM. The cells were plated on a sterile coverslip, supplemented with enriched medium, incubated at 37°C and 10% CO_2, and used on the same day.

Amperometry and measurement of intracellular calcium concentration. Catecholamine release from mouse chromaffin cells was measured in Ringer solution consisting of (in mM): 130 NaCl; 4 KCl; 2 $CaCl_2$; 1 $MgCl_2$; 48 glucose; and 10 HEPES. The pH was adjusted to 7.3 using NaOH. Cells were maintained at 36°C during the experiment. For stimulation of catecholamine release, 10 μM acetylcholine was added. Amperometric fibers were purchased from HEKA (carbon fiber electrode CFE-1, ALA Scientific Instruments). Fibers were clamped to +800 mV, and the tip of the fiber was pressed gently against the cell wall. Currents were recorded using an EPC10 amplifier (HEKA) and acquired with Patchmaster software (HEKA; sample rate 10 kHz, filtering 5 kHz). Amperometric signals were analyzed with IGOR software (WaveMetrics), restricting the analysis to spikes whose amplitudes were at least 5 times larger than the current noise amplitude (48). The intracellular calcium concentration was measured in parallel, using a filter wheel and

a photomultiplier connected to the EPC10. Cells were loaded with Fura-2 by incubation for 20 minutes at 37°C in the incubation medium containing 2 μM Fura-2–acetoxymethyl ester. For the measurement of intracellular calcium concentration, fluorescence at 510 nm was measured during excitation at 340 nm and 380 nm. Fluorescence measurements were acquired with Patchmaster software (HEKA) and analyzed in Origin (Microcal Inc.).

Ultrastructural analysis. Mice were anesthetized with avertin and perfused transcardially with PBS, followed by fixative containing 1% glutaraldehyde and 1% formaldehyde in 0.1 M cacodylate buffer. The adrenal glands were osmicated for 120 minutes using 2% osmium tetroxide in cacodylate buffer, rinsed in water, and dehydrated in an ascending gradient of alcohols followed by acetone and an ascending acetone/Epon gradient. After polymerization in Epon-812 for 48 hours at 60°C, ultrathin sections of 75 nm were cut and contrasted with uranyl acetate and lead citrate solutions. The sections were examined on a transmission electron microscope (Tecnai Biotwin 120) at 2,900- and 9,300-fold magnifications. Randomly chosen cells of the adrenal medullae from 3 independent WT and *Trpm4*$^{-/-}$ animals were photographed and analyzed with AxioVison software (version 4.8.1, AutoMeasure, Zeiss). To estimate the vesicular content in the chromaffin cells, sections with well-fixed cellular constituents were randomly chosen. We analyzed the total area of vesicles in relation to the cell size and the relative frequency distribution of the vesicular size in both genotypes

Statistics. Data are presented as mean ± SEM of *n* independent experiments, unless otherwise stated. Origin 7.0 software (OriginLab) was used for statistical analysis. Significance was assessed with the 2-tailed Student's *t* test unless otherwise indicated. A *P* value less than 0.05 was considered significant.

Acknowledgments

We thank S. Buchholz, K. Fischer, S. Schmidt, C. Matka, C. Wesely, and M. Simon-Thomas for expert technical assistance. This work was supported by the Deutsche Forschungsgemeinschaft (M. Freichel, V. Flockerzi, and F. Schweda); Fonds der Chemischen Industrie and Sander-Stiftung (V. Flockerzi); Forschungsausschuss, the "HOMFOR" program, and Forschungsausschuss der Universität des Saarlandes (M. Freichel, V. Flockerzi); and the Belgian Federal Government (Interuniversity Poles of Attraction Program [IUAP] P6/28), the Research Foundation–Flanders (FWO; G.0565.07, G.0761.10, and KAN1.5.206.09), and the Research Council of the KU Leuven (GOA/09/12, START1/09/046, and EF/95/010) (R. Vennekens, B. Nilius).

Received for publication October 5, 2009, and accepted in revised form June 23, 2010.

Address correspondence to: Marc Freichel, Experimentelle und Klinische Pharmakologie und Toxikologie, Universität des Saarlandes, D-66421 Homburg, Germany. Phone: 49.6841.16.26438; Fax: 49.6841.16.26402; E-mail: marc.freichel@uks.eu.

1. Cowley AW Jr. The genetic dissection of essential hypertension. *Nat Rev Genet*. 2006;7(11):829–840.
2. Hsu HH, et al. Hypertension in mice lacking the CXCR3 chemokine receptor. *Am J Physiol Renal Physiol*. 2009;296(4):F780–F789.
3. Nilius B, Owsianik G, Voets T, Peters JA. Transient receptor potential cation channels in disease. *Physiol Rev*. 2007;87(1):165–217.
4. Inoue R, et al. Transient receptor potential channels in cardiovascular function and disease. *Circ Res*. 2006;99(2):119–131.
5. Montell C, Birnbaumer L, Flockerzi V. The TRP channels, a remarkably functional family. *Cell*. 2002;108(5):595–598.
6. Freichel M, et al. Functional role of TRPC proteins in native systems: implications from knockout and knock-down studies. *J Physiol*. 2005;567(pt 1):59–66.
7. Lange I, Yamamoto S, Partida-Sanchez S, Mori Y, Fleig A, Penner R. TRPM2 functions as a lysosomal Ca2+-release channel in beta cells. *Sci Signal*. 2009;2(71):ra23.
8. Flockerzi V. An introduction on TRP channels. *Handb Exp Pharmacol*. 2007;(179):1–19.
9. Dietrich A, Chubanov V, Kalwa H, Rost BR, Gudermann T. Cation channels of the transient receptor potential superfamily: their role in physiological and pathophysiological processes of smooth muscle cells. *Pharmacol Ther*. 2006;112(3):744–760.
10. Earley S, Gonzales AL, Crnich R. Endothelium-dependent cerebral artery dilation mediated by TRPA1 and Ca2+-activated K+ channels. *Circ Res*. 2009;104(8):987–994.
11. Dietrich A, et al. TRPC6 deficient mice develop an elevated blood pressure and an early onset of the myogenic tone in cerebral arteries. *Naunyn Schmiedebergs Arch Pharmacol*. 2004;369(suppl 1):R61.
12. Pacher P, Batkai S, Kunos G. Haemodynamic profile and responsiveness to anandamide of TRPV1 receptor knock-out mice. *J Physiol*. 2004;558(pt 2):647–657.
13. Suzuki M, Mizuno A, Kodaira K, Imai M. Impaired pressure sensation in mice lacking TRPV4. *J Biol Chem*. 2003;278(25):22664–22668.
14. Zhang DX, et al. Transient receptor potential vanilloid type 4-deficient mice exhibit impaired endothelium-dependent relaxation induced by acetylcholine in vitro and in vivo. *Hypertension*. 2009;53(3):532–538.
15. Vriens J, et al. Modulation of the Ca2 permeable cation channel TRPV4 by cytochrome P450 epoxygenases in vascular endothelium. *Circ Res*. 2005;97(9):908–915.
16. Loot AE, Popp R, Fisslthaler B, Vriens J, Nilius B, Fleming I. Role of cytochrome P450-dependent transient receptor potential V4 activation in flow-induced vasodilatation. *Cardiovasc Res*. 2008;80(3):445–452.
17. Saliez J, et al. Role of caveolar compartmentation in endothelium-derived hyperpolarizing factor-mediated relaxation: Ca2+ signals and gap junction function are regulated by caveolin in endothelial cells. *Circulation*. 2008;117(8):1065–1074.
18. Hartmannsgruber V, et al. Arterial response to shear stress critically depends on endothelial TRPV4 expression. *PLoS ONE*. 2007;2(9):e827.
19. Launay P, Fleig A, Perraud AL, Scharenberg AM, Penner R, Kinet JP. TRPM4 is a Ca2+-activated nonselective cation channel mediating cell membrane depolarization. *Cell*. 2002;109(3):397–407.
20. Nilius B, et al. Voltage dependence of the Ca2+-activated cation channel TRPM4. *J Biol Chem*. 2003;278(33):30813–30820.
21. Xu XZ, Moebius F, Gill DL, Montell C. Regulation of melastatin, a TRP-related protein, through interaction with a cytoplasmic isoform. *Proc Natl Acad Sci U S A*. 2001;98(19):10692–10697.
22. Liu D, Liman ER. Intracellular Ca2+ and the phospholipid PIP2 regulate the taste transduction ion channel TRPM5. *Proc Natl Acad Sci U S A*. 2003;100(25):15160–15165.
23. Hofmann T, Chubanov V, Gudermann T, Montell C. TRPM5 is a voltage-modulated and Ca(2+)-activated monovalent selective cation channel. *Curr Biol*. 2003;13(13):1153–1158.
24. Vennekens R, et al. Increased IgE-dependent mast cell activation and anaphylactic responses in mice lacking the calcium-activated nonselective cation channel TRPM4. *Nat Immunol*. 2007;8(3):312–320.
25. Gerzanich V, et al. De novo expression of Trpm4 initiates secondary hemorrhage in spinal cord injury. *Nat Med*. 2009;15(2):185–191.
26. Earley S, Waldron BJ, Brayden JE. Critical role for transient receptor potential channel TRPM4 in myogenic constriction of cerebral arteries. *Circ Res*. 2004;95(9):922–929.
27. Demion M, Bois P, Launay P, Guinamard R. TRPM4, a Ca2+-activated nonselective cation channel in mouse sino-atrial node cells. *Cardiovasc Res*. 2007;73(3):531–538.
28. Kruse M, et al. Impaired endocytosis of the ion channel TRPM4 is associated with human progressive familial heart block type I. *J Clin Invest*. 2009;119(9):2737–2744.
29. Guinamard R, Demion M, Magaud C, Potreau D, Bois P. Functional expression of the TRPM4 cationic current in ventricular cardiomyocytes from spontaneously hypertensive rats. *Hypertension*. 2006;48(4):587–594.
30. Van Vliet BN, Chafe LL, Montani JP. Characteristics of 24 h telemetered blood pressure in eNOS-knockout and C57Bl/6J control mice. *J Physiol*. 2003;549(pt 1):313–325.
31. Luscher TF, Barton M. Biology of the endothelium. *Clin Cardiol*. 1997;20(11 suppl 2):II-3–II-10.
32. Davis MJ, Hill MA. Signaling mechanisms underlying the vascular myogenic response. *Physiol Rev*. 1999;79(2):387–423.
33. Okunishi H, Miyazaki M, Toda N. Evidence for a putatively new angiotensin II-generating enzyme in the vascular wall. *J Hypertens*. 1984;2(3):277–284.
34. Li M, et al. Involvement of chymase-mediated angiotensin II generation in blood pressure regulation. *J Clin Invest*. 2004;114(1):112–120.
35. Esler M, et al. Sympathetic nerve biology in essential hypertension. *Clin Exp Pharmacol Physiol*. 2001;28(12):986–989.
36. Guyenet PG. The sympathetic control of blood pressure. *Nat Rev Neurosci*. 2006;7(5):335–346.
37. Lein ES, et al. Genome-wide atlas of gene expression in the adult mouse brain. *Nature*. 2007;445(7124):168–176.
38. Grabner CP, Price SD, Lysakowski A, Fox AP. Mouse chromaffin cells have two populations of dense core vesicles. *J Neurophysiol*. 2005;94(3):2093–2104.
39. Lapointe JY, Bell PD, Sabirov RZ, Okada Y. Calcium-activated nonselective cationic channel in macula densa cells. *Am J Physiol Renal Physiol*.

2003;285(2):F275–F280.
40. Sharif-Naeini R, et al. TRP channels and mechanosensory transduction: insights into the arterial myogenic response. *Pflugers Arch*. 2008;456(3):529–540.
41. Krapivinsky G, Mochida S, Krapivinsky L, Cibulsky SM, Clapham DE. The TRPM7 ion channel functions in cholinergic synaptic vesicles and affects transmitter release. *Neuron*. 2006;52(3):485–496.
42. Mills PA, et al. A new method for measurement of blood pressure, heart rate, and activity in the mouse by radiotelemetry. *J Appl Physiol*. 2000; 88(5):1537–1544.
43. Skryabin BV, et al. Hypervolemic hypertension in mice with systemic inactivation of the (floxed) guanylyl cyclase-A gene by alphaMHC-Cre-mediated recombination. *Genesis*. 2004;39(4):288–298.
44. Ritthaler T, Schricker K, Kees F, Kramer B, Kurtz A. Acute hypoxia stimulates renin secretion and renin gene expression in vivo but not in vitro. *Am J Physiol*. 1997;272(4 pt 2):R1105–R1111.
45. Schweda F, Wagner C, Kramer BK, Schnermann J, Kurtz A. Preserved macula densa-dependent renin secretion in A1 adenosine receptor knockout mice. *Am J Physiol Renal Physiol*. 2003;284(4):F770–F777.
46. Wagner C, de Wit C, Kurtz L, Grunberger C, Kurtz A, Schweda F. Connexin40 is essential for the pressure control of renin synthesis and secretion. *Circ Res*. 2007;100(4):556–563.
47. Weissgerber P, et al. Reduced cardiac L-type Ca2+ current in Ca(V)beta2–/– embryos impairs cardiac development and contraction with secondary defects in vascular maturation. *Circ Res*. 2006; 99(7):749–757.
48. Mosharov EV, Sulzer D. Analysis of exocytotic events recorded by amperometry. *Nat Methods*. 2005;2(9):651–658.